

Quantitative Morphometry of Hippocampal Pyramidal Cells: Differences between Anatomical Classes and Reconstructing Laboratories

RUGGERO SCORCIONI,¹ MACIEJ T. LAZAREWICZ,² AND GIORGIO A. ASCOLI^{1,3*}

¹Krasnow Institute for Advanced Study, George Mason University, Fairfax, Virginia 22030

²Department of Bioengineering, University of Pennsylvania, Philadelphia, Pennsylvania 19104

³Psychology Department, George Mason University, Fairfax, Virginia 22030

ABSTRACT

The dendritic trees of hippocampal pyramidal cells play important roles in the establishment and regulation of network connectivity, synaptic plasticity, and firing dynamics. Several laboratories routinely reconstruct CA3 and CA1 dendrites to correlate their three-dimensional structure with biophysical, electrophysiological, and anatomical observables. To integrate and assess the consistency of the quantitative data available to the scientific community, we exhaustively analyzed 143 completely reconstructed neurons intracellularly filled and digitized in five different laboratories from 10 experimental conditions. Thirty morphometric parameters, including the most common neuroanatomical measurements, were extracted from all neurons. A consistent fraction of parameters (11 of 30) was significantly different between CA3 and CA1 cells. A considerably large number of parameters was also found that discriminated among neurons within the same morphological class, but reconstructed in different laboratories. These interlaboratory differences (8 of 30 parameters) far outweighed the differences between experimental conditions within a single lab, such as aging or preparation method (at most two significant parameters). The set of morphometrics separating anatomical regions and that separating reconstructing laboratories were almost entirely nonoverlapping. CA3 and CA1 neurons could be distinguished by global quantities such as branch order and Sholl distance. Differences among laboratories were largely due to local variables such as branch diameter and local bifurcation angles. Only one parameter (a ratio of branch diameters) separated both morphological classes and reconstructing laboratories. Compartmental simulations of electrophysiological activity showed that both differences between anatomical classes and reconstructing laboratories could dramatically affect the firing rate of these neurons under different experimental conditions. *J. Comp. Neurol.* 473:177–193, 2004. © 2004 Wiley-Liss, Inc.

Indexing terms: branching; comparative analysis; computational models; dendritic structure; hippocampus; pyramidal cells; three-dimensional reconstructions

CA3 and CA1 pyramidal cells are prominent players in all theories of hippocampal function in learning, memory, and spatial representation (e.g., Marr, 1971; Buzsaki, 1989; Gluck, 1996; Levy, 1996; McNaughton et al., 1996; Rolls, 1996; Hasselmo and Wyble, 1997; Shapiro and Eichenbaum, 1999), with their dendrites integrating input from converging pathways. Dendritic structure is altered in common neuropathologic conditions, including epilepsy (Scheibel, 1980; Swann et al., 2000), Alzheimer's disease (Anderton et al., 1998; Bulinski et al., 1998), and Fragile X dementia (Kaufmann and Moser, 2000; Irwin et al., 2002). Dendritic morphology has been also quantitatively investigated in relation to postnatal development (Pokorny and Yamamoto, 1981; Duffell et al., 2000), aging (Pyapali and Turner, 1996; Wasowicz et al., 1996), lesions (Pyapali and

Turner, 1994; Colling et al., 1996), learning (Collin et al., 1997; Muller et al., 2002), synaptic connectivity (Desmond

Grant sponsor: National Institutes of Health R01; Grant number: NS39600 (G.A.A.); Grant sponsor: National Institute of Neurological Disorders and Stroke; Grant sponsor: National Institute of Mental Health; Grant sponsor: National Science Foundation.

*Correspondence to: Giorgio A. Ascoli, Krasnow Institute (MS 2A1), George Mason University, 4400 University Drive, Fairfax, VA 22030. E-mail: Ascoli@gmu.edu

Received 26 August 2003; Revised 22 October 2003; Accepted 15 December 2003

DOI 10.1002/cne.20067

Published online in Wiley InterScience (www.interscience.wiley.com).

TABLE 1. Summary of Digitized Three-Dimensional Reconstructions of Hippocampal Pyramidal Cells¹

	Archive	Region	#	Strain	Age (mo)	Sex	Preparation	Reference
A1	Amaral	CA1	19	SD	1–2	F	In vitro	Ishizuka et al., 1995
C1	Claiborne	CA1	7	SD	2–12	6M, 1F	In vitro	Carnevale et al., 1997
G1	Gulyas	CA1	18	Wi	1–2	M	In vitro	Megias et al., 2001
T1								
T1.old	Turner	CA1	15	F344	22–24	M	In vitro	Pyapali and Turner, 1996
T1.young	Turner	CA1	10	F344	2	M	In vitro	Pyapali et al., 1998
T1.vivo	Turner	CA1	24	SD	2–8	M	In vivo	Pyapali et al., 1998
A3	Amaral	CA3	20	SD	1–2	F	In vitro	Ishizuka et al., 1995
C3	Claiborne	CA3	4	SD	1–2	F	In vitro	Carnevale et al., 1997
B3	Barrionuevo	CA3	8	SD	1	M	In vitro	Henze et al., 1996
T3	Turner	CA3	18	SD, Wi	2–8	F,M	In vivo	Turner et al., 1995

¹Rows and columns correspond to different groups of neurons and their characteristics, respectively.

and Levy, 1997), stereology (Fiala and Harris, 2001), neurogenesis (Shetty and Turner, 1995), and electrophysiology (Bilkey and Schwartzkroin, 1990; Larkman and Mason, 1990).

With the advent of software for anatomically detailed simulations of neuronal biophysics, computational models have repeatedly suggested that dendritic morphology may affect pyramidal cell physiology, including electrotonic properties (Carnevale et al., 1997), action potential back-propagation (Vetter et al., 2001), firing patterns (Krichmar et al., 2002), synaptic integration (Poirazi et al., 2003), and coincidence detection (Schaefer et al., 2003). In addition, quantitative morphological data have been used in computational models of dendritic structure (Donohue et al., 2002; Samsonovich and Ascoli, 2003).

This continuous interest in cellular morphology and the extensive time required for dendritic reconstructions have encouraged the practice of data sharing (Gardner et al., 2003). Hundreds of completely reconstructed neurons have been made available in digital format (reviewed in Ascoli, 2002). Arbitrarily selected subsets of these data have been already (re)used in follow-up studies by the same and other research groups (Migliore et al., 1995; Cannon et al., 1999; Vetter et al., 2001; Lazarewicz et al., 2002b). Several distinct experimental protocols were used to produce these data. However, almost each publication characterizes dendritic morphology with different sets of measurements, making a direct comparison across data sets problematic.

The present report focuses on the publicly available CA3 and CA1 data sets (amounting to 143 complete cells), which correspond to seven studies published between 1995 and 2001 by five distinct laboratories (see Materials and Methods section). To integrate and assess the consistency of these data, we extracted an exhaustive array of morphometric parameters directly from the raw digital files of the three-dimensional reconstructions. The parameters were chosen to include most measurements commonly adopted in the literature. Here, we report the resulting statistical analysis, which indicates that the differences among sets of neurons reconstructed from different laboratories are as considerable as those observed between morphological classes. In addition, we show that the morphometric parameters that discriminate among laboratories (across morphological classes) and those that discriminate between CA3 and CA1 pyramidal cells (independent of the reconstructing laboratories) constitute geometrically separate and distinct sets, which can differen-

tially affect the simulated electrophysiological behavior of hippocampal neurons.

MATERIALS AND METHODS

A total of 143 intracellularly labeled and completely reconstructed pyramidal neurons from the rat hippocampus were collected from five laboratories (Table 1). The first data sets consisted of 20 CA3 and 19 CA1 cells from the laboratory of David Amaral at the University of California at Davis (A3 and A1, respectively, in Table 1). These cells were injected with horseradish peroxidase in the thick slice (“in vitro”) preparation, reconstructed by using the Eutectic Neuron Tracing system (Capowski, 1983), and extensively described (Ishizuka et al., 1995). Digitized files were obtained directly from the authors and are now publicly available (with permission of the authors) at www.krasnow.gmu.edu/L-Neuron (case-sensitive).

The second, more heterogeneous group of neurons was provided by the laboratory of Dennis Turner at Duke University. Eighteen CA3 pyramidal cells (T3 in Table 1) were injected with biocytin in whole anesthetized animals (“in vivo”), serially reconstructed using Microbrightfield NeuroLucida (Glaser and Glaser, 1990), and statistically analyzed (Turner et al., 1995). The same preparation was used to trace 24 CA1 pyramidal cells (T1.vivo in Table 1, see Pyapali et al., 1998). A different set of 15 CA1 pyramidal cells from 2-year-old rats (T1.old) were labeled with neurobiotin in vitro and reconstructed with NeuroLucida (Pyapali and Turner, 1996). Finally, a control group of 10 CA1 pyramidal cells was also available in an identical preparation of 2-month-old rats from the same study (T1.young). Digitized files of all of these neurons can be obtained from the Duke-Southampton archive of neuronal morphology at <http://neuron.duke.edu/cells/cellArchive.html> (Cannon et al., 1998).

A third group of pyramidal cells was collected in Brenda Claiborne’s laboratory at the University of Texas at San Antonio (Carnevale et al., 1997). This set consists of seven CA1 and four CA3 neurons (C1 and C3, respectively, in Table 1) collected with the same experimental procedure as for the Amaral cells. These cells are available as digital files at www.utsa.edu/claibornelab. The fourth data set consists of 18 pyramidal cells, exclusively from area CA1, from the group of Attila Gulyas at the Hungarian Academy of Sciences (Megias et al., 2001). These cells (G1), available at www.koki.hu/~gulyas/ca1cells/cellfiles.html,

were injected with biotinylated dextran amine in vivo and serially reconstructed with the ARBOR program (Wolf et al., 1995). Finally, the last data set included 8 CA3 pyramidal cells from the laboratory of German Barrionuevo at the University of Pittsburgh (Henze et al., 1996). These cells were labeled with neurobiotin in vitro and reconstructed with Eutectic (B3 in Table 1).

In summary, 93 of 143 cells (65%) are from CA1, and 50 (35%) are from CA3. Sixty cells (42%) were recovered from whole animals injections (“in vivo” preparation), with the other 83 (58%) injected after slicing (“in vitro” preparation). Seventy-nine cells (55%) were from young animals (1–2 months), 49 (34%) from adults (2–12 months), and the remaining 15 (11%) from aged rats (22–24 months). Additional experimental variables reported in Table 1 include the rat strain and sex. This information, however, is partly incomplete for the T3 group. Excluding these cells, 44 of the remaining 125 neurons (35%) were from females and 81 (65%) from males. Eighty-two neurons (66%) came from Sprague-Dawley rats, 18 (14%) from Wistar, and 25 (20%) from Fischer 344. The two-dimensional projections of two samples from each of the neuronal groups summarized in Table 1 are shown in Figure 1.

The original anatomical files from all data sets consisted of a list of the three-dimensional coordinates and diameter of each traced point, its tag (soma, basal dendrite, apical dendrite, or axon), and its downstream connectivity with two other points (bifurcation), one (continuation), or none (termination). This information was expressed in the various data sets in a variety of formats, mostly depending on the reconstruction system. Turner’s and Gulyas’ files (T1, T3, and G1) were in SWC format, Amaral’s and Barrionuevo’s in Eutectic, and Claiborne’s in a variation of the Eutectic format (for a description of formats, see Ascoli et al., 2001). All morphologic measurements were extracted from the anatomical files by using the L-Measure software (Scorcioni and Ascoli, 2001), which is publicly available at www.krasnow.gmu.edu/L-Neuron (case-sensitive). L-Measure allows the automated extraction of multiple sets of neuroanatomical parameters from different groups of reconstructed neurons in any of the known file formats used in the neuroanatomical community.

Because only a small proportion of the available neurons included either partial or full reconstructions of the axon, only the soma and the dendritic trees (basal and apical separately as well as jointly) were considered. The morphometric parameters analyzed in this study are listed in Table 2. We call a *tree* the part of the neuron structure exiting the soma from a single point (*tree stem*). A *branch* is the part of a tree between two consecutive *nodes* (bifurcations, terminations, tree stems). A *compartment* is the part of a branch between two consecutive tracing points, and it represents the smallest neuronal element in the reconstruction. The parameters used to statistically characterize the morphology of pyramidal cells were defined through an exhaustive analysis of the relevant neurobiological literature since the commercial development of computer-assisted reconstruction systems starting from 1985. This set of parameters was selected to include the majority of measurements typically reported in peer-reviewed publications of quantitative studies of single neuron anatomy.

Several parameters characterized the overall geometry of the whole neuron, such as the height, width, and depth of the arborization, the total dendritic length and internal

volume, and the fractal dimension. The classic “relational” property of branch number vs. path distance (Sholl-like diagrams) was captured by the average branch distance (“Sholl distance” in Table 2), which could be included in simple statistical analyses. Individual tree properties were also included, such as maximum number of tips per stem and the maximum distances (Euclidian and along the path) between the soma and a dendritic termination. Other parameters concerned the topology of the branching patterns, including the number of trees and bifurcations, the partition asymmetry, and the maximum branch order. Average branch and bifurcation properties were captured by bifurcation angles, contraction or dendritic meandering, average branch length, taper rates, and bifurcation diameter ratios between parent and daughter and between the two daughters. Of the 30 parameters, 18 were independent of diameter measurement (top part of Table 2). This distinction is relevant in light of the possible limited precision in the experimental determination of small diameter values reported by the authors in two of the studies (Ishizuka et al., 1995; and www.utsa.edu/claibornelab).

All statistical comparisons presented in this study were performed by pair-wise analysis. The number of neurons in each group was relatively small (14.3 ± 6.3), and the shape of the parameter distributions was skewed and generally not Gaussian (see, e.g., Fig. 2). Thus, the Wilcoxon rank sum test was used instead of the more common Student *t* test. Corresponding *P* values were calculated with the *ranktest* function in Matlab (The MathWorks, Natick, MA, v. R11). Because each comparison between two neuronal groups used all 30 morphometric measurements, the Bonferroni correction was applied (i.e., all Wilcoxon *P* values were multiplied by 30). Corresponding *P* values are reported as ≥ 1 if corrected to a value out of the 0 to 1 range. Note that, given the large number of partially interdependent parameters, the choice of the Bonferroni correction is particularly conservative. Use of less stringent correction criteria, such as the False Discovery Rate (Benjamini and Hochberg, 1995) would result in smaller *P* values throughout the study.

Electrophysiological simulations were run in NEURON version 5.4 (Hines and Carnevale, 1997) on a Pentium Xeon computer under the Red Hat Linux operating system. Morphological files were preprocessed by merging all adjacent compartments with the same diameter within a branch into single sections (Lazarewicz et al., 2002a). Sections were then divided in several segments of length no greater than one tenth of the length constant at 100 Hz (Hines and Carnevale, 2001). Simulations were run with a fixed time step of 25 μ sec.

The biophysical model was constructed primarily based on the work of Vetter et al. (2001). Two similar models, only differing in the kinetic equations, are made available by these authors through the internet (www.dendrite.org). We adopted the variant based on the equations by Paré et al. (1998). In these models, all biophysical properties are uniformly distributed over the membrane, allowing for the direct detection of the electrophysiological consequence of morphological differences. In addition, dendrites are endowed in these models with voltage-gated currents, consistent with the active properties of hippocampal pyramidal neurons. In particular, membranes contained passive elements as well as fast sodium and potassium delay rectifier currents (I_{Na} and I_{Kdr}). All passive properties and

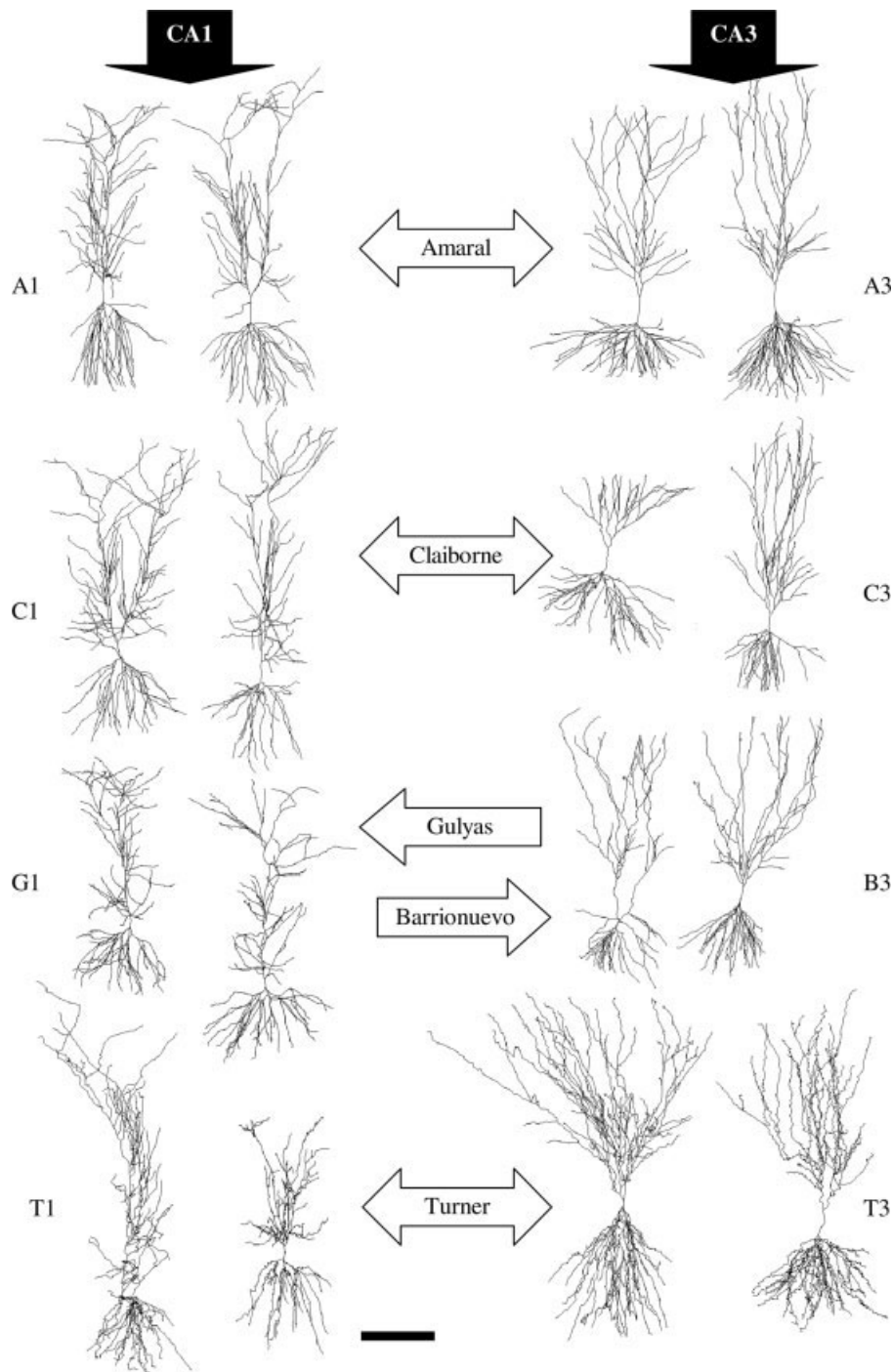


Fig. 1. Two-dimensional graphic representation of 16 hippocampal pyramidal cells. From top left: Amaral (c10261 and c11563, CA1; c10861 and c62563, CA3); Claiborne (5038801 and 8228804a, CA1;

11199101 and 2109201, CA3); Gulyas (pc1a and pc2b, CA1), Barrionuevo (cell1zr and cell8zr, CA3); Turner (n175t and n122t, CA1; l160atr and l48bt, CA3). Scale bar = 200 μm .

current densities had constant values over the soma and all dendrites of each neuron. As in the model by Vetter et al. (2001), the capacitance (C_m), axial resistance (R_i), membrane resistance (R_m), and passive reverse potential (E_{leak}) were assigned values of 1 $\mu\text{F}/\text{cm}^2$, 150 Ωcm , 12,000

Ωcm^2 , and -70 mV, respectively. Sodium and potassium reversal potentials (E_{Na} and E_{K}) were also set as in the original model to 60 mV and -90 mV, respectively (Vetter et al., 2001). In contrast, the values of the peak conductances ($g_{\text{Na,max}}$ and $g_{\text{Kdr,max}}$) were slightly modified (to

TABLE 2. Definitions of Morphometric Parameters

Height (μm)	Neuronal height of a box containing 95% of the compartments
Width (μm)	Neuronal width of a box containing 95% of the compartments
Depth (μm)	Neuronal depth of a box containing 95% of the compartments
Total length (μm)	Total extension of the dendritic arborization
Bifurcations	Number of bifurcations
Branches	Number of branches
Trees	Number of dendritic trees stemming from the soma
Max tips	Maximum number of tree terminals per neuron
Hausdorff	Fractal dimension computed with the box counting method
Max distance (μm)	Euclidean distance between the soma and the farthest compartment
Max path distance (μm)	Distance along the dendrite between the soma and the farthest terminal tips
Sholl distance (μm)	Average Euclidean distance of a compartment from the soma
Topological asymmetry	Average partition over all bifurcations. Partition is computed at every bifurcation, and it is defined as $\frac{ r-l }{r+l-2}$, where r and l are the number of terminations of the two daughter trees
Max branch order	Max number of bifurcations between soma and terminal tips
Local bifurcation angle (°)	Average of the angles between the two immediate daughters at each bifurcation
Remote bifurcation angle (°)	Average of the angles between the lines joining each bifurcation with first node (a node is defined as a bifurcation, termination point, or tree stem) in each of the two daughters
Branch length (μm)	Average length of all branches
Contraction	Average ratio between the Euclidean distance and the distance along the path between two consecutive nodes; this parameter (range 0–1) captures the meandering, or wiggling, of dendritic path: a unitary value corresponds to perfectly straight branches, while increasing “zigzags” result in lower values
Dendritic volume (μm ³)	Total internal volume of the dendritic arborization
Dendritic surface (μm ²)	Total surface area of the dendritic arborization
Soma surface (μm ²)	Surface area of the soma. If the soma is defined as a single compartment, then a spherical assumption is made, otherwise the soma surface is computed as the sum of external surface of all compartments forming the soma
Diameter (μm)	Average diameter over all compartments
Last bifurcation diameter (μm)	Average diameter of parent of the last bifurcation; a bifurcation is defined as ‘last’ when it only leads to two terminal branches
Diameter threshold (μm)	Average value below which no bifurcation is found; calculated as the weighted average of last bifurcation diameter (50%) and the two daughters’ diameter (each 25%)
Daughter ratio	Average diameter ratio of the two daughters over all bifurcations
Parent–child ratio	Average diameter ratio between parent and daughter diameter over all bifurcations
Rall’s power	Best fitting parameter n for Rall’s formula: $d_p^n = d_1^n + d_2^n$, where d_p , d_1 , d_2 , are the parent diameter and the two daughter diameter
Power correction	A measure of how far the bifurcation is from the ideal value of a Rall’s power (¾). Calculated as $\frac{D_p^3}{D_1^3 + D_2^3}$; it provides a measure of how close/far the bifurcation is to the perfect Rall bifurcation behavior
Branch taper rate	Average taper rate per branch, calculated as the difference between final and initial diameter divided by the initial diameter at each branch
Unit taper rate	Average taper rate per unit length. Calculated as the difference between final and initial diameter divided by the branch length

135 pS/μm² and 150 pS/μm², respectively) to ensure sustained firing. I_{Na} and I_{Kdr} were calculated according to the following formulas (Paré et al., 1998; www.dendrite.org/dendritica-1.0/batch_back/back/mod/kvd_nad):

$$I_{Na} = g_{Na,max} m^3 h (\nu - E_{Na}), \quad I_{Kdr} = g_{Kdr,max} n^4 (\nu - E_K)$$

$$\frac{dx}{dt} = \frac{x_\infty - x}{\tau_x}, \quad x_\infty = \frac{\alpha}{\alpha + \beta}, \quad \tau_x = \frac{1}{\alpha + \beta}, \quad x = m, h, n$$

$$\alpha_m = \frac{-0.32(50 + \nu)}{e^{-\frac{50 + \nu}{4}} - 1}, \quad \alpha_h = 0.128 e^{-\frac{46 + \nu}{18}},$$

$$\alpha_n = \frac{-0.032(48 + \nu)}{e^{-\frac{48 + \nu}{5}} - 1}$$

$$\beta_m = \frac{0.28(\nu + 23)}{e^{-\frac{\nu + 23}{5}} - 1}, \quad \beta_h = \frac{4}{e^{-\frac{23 + \nu}{5}} + 1}, \quad \beta_n = 0.5 e^{-\frac{53 + \nu}{40}}$$

Firing frequencies were measured for 1 second under somatic current clamp. In the non-normalized protocol, the current injection was 0.55 nA for all neurons. In the normalized protocol, the current injection was 6.5 nA divided by the somatic impedance value at 100 Hz (in MΩ), measured separately for each neuron with the corresponding built-in NEURON function. The values of 0.55 and 6.5 nA constituted an empirical balance to maximize the number of neurons that would fire at least one spike in both protocols, while preventing any neuron from excessive excitation that would lead to subthreshold oscillations.

Firing rate–injected current (f-I) relationships were measured by stimulating neurons with current injections around the above normalized value. Fifty data points were collected for a sample of neurons, showing that the f-I relationship was highly linear ($R > 0.95$) around a relatively broad range of stimuli (50–150% of the above normalized value). Thus, three data points (at 90%, 100%, and 110%) were plotted for each neuron to calculate the f-I slope (or gain) and intercept (shift) by linear regression.

Finally, in two sets of experiments, dendritic diameter was normalized either additively or multiplicatively, using the neuronal group with the largest average diameter value (T3) as reference. In the first case, the difference between the average reference diameter and the average diameter of the given class was added to all diameter values of neurons of each class. In the second case, all diameter values of neurons of each class were multiplied by the ratio between the average reference diameter and the average diameter of the given class.

RESULTS

Multiple pair-wise comparisons were carried out on groups of neurons with similar attributes. For example, the T1.vivo group (CA1 pyramidal cells injected in live Sprague-Dawley rats and reconstructed in Turner’s laboratory) was compared with T1.young (same cell class and laboratory, but injected in slices and from a different rat strain), to T3 (same laboratory and injection method, but different morphological class, CA3), and to G1 (same morphological class and injection method, but different laboratory). Only one morphometric parameter, width, was different between the in vivo preparation from Sprague-Dawley rats and the in vitro preparation from Fischer rats (Fig. 2), confirming previous reports (Pyapali et al., 1998). Similarly, the comparison between dendritic morphology in young adults and aged rats from the same laboratory

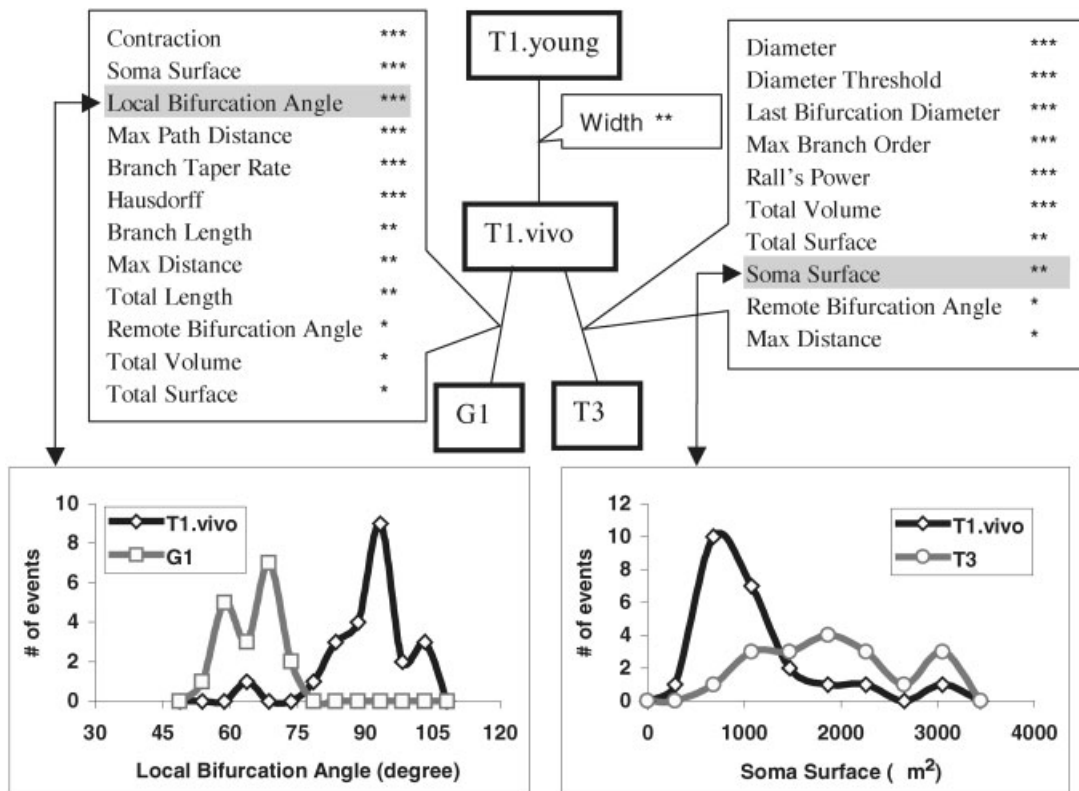


Fig. 2. Pair-wise comparison schema with significantly different parameters listed in corresponding arrowed boxes. The bottom plots show the detailed distributions of two different parameters. *, $P \leq 0.05$; **, $P \leq 0.01$; ***, $P \leq 0.001$.

and preparation (T1.young vs. T1.old) only yielded statistical differences in total dendritic length and arbor width (in agreement with the analysis of Pyapali et al., 1996), with even these two parameters falling to nonsignificant values after Bonferroni correction (not shown). In contrast, and as expected, a large number of morphometric parameters, including maximum branching order, total dendritic volume, remote bifurcation angle, and maximum distance from soma to tips, were found to be significantly different between CA3 and CA1 pyramidal cells (Fig. 2).

More surprisingly, an even greater number of parameters (more than one third of all measurements) discriminated between the morphologies of neurons from the same cell class and same preparation type but reconstructed in different laboratories (T1.vivo vs. G1). This set included such parameters as contraction, local bifurcation angle, and several diameter-related measurements. Examples of the statistical distributions for two parameters are also shown in Figure 2. To appreciate the consistency of the differences between groups relative to the intrinsic variability within each group, the complete list of mean and standard deviations of all parameters for these four neuronal groups is reported in Table 3.

A more extended pair-wise comparison of the available neuronal groups is presented in summary form in Figure 3. Differences between groups included morphological class in two cases (A1 vs. A3 and T1.vivo vs. T3), reconstructing laboratory in four cases (T1.vivo vs. G1, T1.young vs. A1, A3 vs. B3, and A1 vs. C1), preparation

method in one case (T1.young vs. T1.vivo), rat strain in 3 cases (T1.young vs. T1.vivo, T1.vivo vs. G1, and T1.young vs. A1), and age in four cases (T1.young vs. T1.vivo, T1.old vs. T1.young, T1.vivo vs. G1, and A1 vs. C1). Most parameters (25 of 30) showed statistically significant differences in at least one of the pair-wise comparisons, and several parameters displayed highly significant differences in as many as four pair-wise comparisons. However, none of the morphometric parameters was significantly different in all of the comparisons (Fig. 3). Thus, for each group difference (morphological class, reconstructing laboratory, preparation method, rat strain, and age), we looked for the parameters that were significant in more than 50% of the relative pair-wise comparisons (i.e., two of two and at least two of three cases for morphological classes and rat strain, respectively, and at least three of four cases for reconstructing laboratories and age). Only two group differences, namely the reconstructing laboratory and the morphological class, could be matched with several morphometric parameters under these criteria. Parameters that systematically uncovered statistical differences between laboratories included contraction, local bifurcation angle, and total dendritic surface. Parameters that systematically returned significant P values between CA3 and CA1 neurons included maximum branch order, remote bifurcation angle, and somatic surface.

To determine the morphological differences between CA3 and CA1 neurons over all reconstructing laboratories and experimental conditions, two groups of neurons were

TABLE 3. Pair-wise Comparisons over All 30 Morphometric Parameters between T1.vivo and T1.young, T1.vivo and T3, and T1.vivo and G1 (as Represented in the Schema of Figure 2)¹

	T1.vivo	T1.young	<i>P</i> value	T3	<i>P</i> value	G1	<i>P</i> value
Local bifurcation angle	88 ± 9.0	89 ± 5.0	≥1	86 ± 9.0	≥1	62 ± 5.0	7.0 · 10 ^{-06***}
Remote bifurcation angle	60 ± 6.0	59 ± 5.0	≥1	50 ± 8.0	0.013*	53 ± 4.0	0.011*
Max branch order	20.5 ± 5.6	22 ± 5.4	≥1	10 ± 2.3	1.4 · 10^{-05***}	23 ± 4.0	≥1
Branch length	110 ± 35	88 ± 10	≥1	110 ± 25	≥1	76 ± 6.0	0.0011**
Contraction	0.77 ± 0.040	0.73 ± 0.060	≥1	0.72 ± 0.074	0.51	0.96 ± 0.0070	2.0 · 10^{-06***}
Daughter ratio	2.0 ± 0.50	1.7 ± 0.40	0.70	1.70 ± 0.32	0.33	1.9 ± 0.15	≥1
Depth	430 ± 270	260 ± 250	0.77	280 ± 100	≥1	380 ± 70	≥1
Diameter threshold	0.53 ± 0.15	0.72 ± 0.30	≥1	0.99 ± 0.27	4.0 · 10^{-06***}	0.41 ± 0.023	0.24
Diameter	0.51 ± 0.17	0.77 ± 0.29	0.26	0.94 ± 0.16	3.0 · 10^{-06***}	0.47 ± 0.031	≥1
Avg distance	250 ± 60	210 ± 38	≥1	210 ± 46	0.47	210 ± 25	0.62
Max distance	750 ± 150	630 ± 150	0.56	570 ± 160	0.014*	600 ± 70	0.0020**
Hausdorff	1.4 ± 0.11	1.5 ± 0.12	≥1	1.5 ± 0.12	0.58	1.2 ± 0.055	2.0 · 10^{-04***}
Height	500 ± 210	650 ± 200	≥1	630 ± 200	≥1	400 ± 100	≥1
Last bifurcation diameter	0.50 ± 0.15	0.71 ± 0.38	≥1	0.91 ± 0.18	8.0 · 10^{-06***}	0.42 ± 0.035	≥1
Total length	17000 ± 6300	16000 ± 4500	≥1	20000 ± 9800	≥1	11000 ± 2300	0.0020**
Bifurcations	82 ± 21	91 ± 26	≥1	87 ± 30	≥1	75 ± 14	≥1
Branches	160 ± 42	190 ± 51	≥1	180 ± 60	≥1	150 ± 28	≥1
Trees	4.0 ± 1.3	4.8 ± 2.4	≥1	5.6 ± 2.0	0.12	4.5 ± 0.86	≥1
Parent-child ratio	0.84 ± 0.058	0.87 ± 0.036	≥1	0.85 ± 0.064	≥1	0.83 ± 0.021	≥1
Topological asymmetry	0.53 ± 0.041	0.55 ± 0.049	≥1	0.48 ± 0.059	0.097	0.52 ± 0.038	≥1
Max path distance	1300 ± 460	1200 ± 200	≥1	1100 ± 470	≥1	810 ± 100	4 · 10^{-05***}
Power correction	1.7 ± 0.14	1.73 ± 0.12	≥1	1.6 ± 0.10	≥1	1.6 ± 0.055	≥1
Rall's power	1.1 ± 0.27	1.3 ± 0.40	≥1	1.7 ± 0.26	2.0 · 10^{-05***}	0.89 ± 0.14	≥1
Soma surface	71 ± 47	86 ± 93	≥1	150 ± 94	0.0070**	4.1 ± 1.6	2.0 · 10^{-06***}
Total surface	28000 ± 15000	38000 ± 23000	≥1	59000 ± 29000	0.0050**	17000 ± 3100	0.037*
Branch taper rate	-0.034 ± 0.031	-0.034 ± 0.025	≥1	-0.060 ± 0.050	0.67	-0.0048 ± 0.0017	1.0 · 10^{-04***}
Unit taper rate	-0.0040 ± 0.0040	-0.0020 ± 0.0050	≥1	-0.0090 ± 0.013	≥1	-0.0030 ± 0.0035	≥1
Max tips	84 ± 21	94 ± 25	≥1	94 ± 33	≥1	78 ± 14	≥1
Total volume	6700 ± 4400	14000 ± 12000	≥1	22000 ± 11500	1.2 · 10^{-04***}	2900 ± 600	0.012*
Width	760 ± 140	440 ± 140	0.003**	590 ± 230	0.76	650 ± 56	0.11

¹Statistically significant parameters are bold.

*→ *P* ≤ 0.05.

**→ *P* ≤ 0.01.

***→ *P* ≤ 0.001.

formed by pooling together data from the Amaral, Turner, and Claiborne sets. In particular, the CA3 group included 42 neurons from both genders, preparation methods (in vitro or in vivo), and two strains (Sprague-Dawley and Wistar) with an age range of 1 to 8 months. The CA1 group was formed by 75 neurons also from both genders, preparation methods, and two strains (Sprague-Dawley and Fisher 344) with an age range of 1 to 24 months. To maintain a more balanced comparison, with respect to possible interlaboratory differences, the Gulyas (CA1 only) and Barrionuevo (CA3 only) data were not included in this analysis (see below for their use as validation sets). Eleven morphometric parameters returned significant differences between the CA3 and the CA1 groups (Table 4), five of which with *P* values below 0.00005. These parameters included the maximum branching order, soma surface, Sholl and maximum path distances, topological asymmetry, and the number of trees, in general agreement with previous reports (e.g., Ishizuka et al., 1995; Cannon et al., 1999), as well as the remote bifurcation angle, parent to child ratio, and Rall's power, which constitute novel observations.

To tease out the morphological differences between reconstructing laboratories as independently as possible from other factors, three groups of neurons were formed by pooling together heterogeneous data solely on the basis of the originating laboratory. The Amaral group consisted of 39 pyramidal cells, nearly half and half from CA3 and CA1. The Turner group consisted of 67 neurons, including all cells from CA3 and CA1 regions, in vivo and in vitro preparations, young and aged animals, and three different strains (Sprague-Dawley, Wistar, and Fischer 344). Finally, the Claiborne group had the smallest sample size (11 total), including both CA3 and CA1 pyramidal cells and a balanced sample of males and females.

The comparison between the Turner and Amaral groups resulted in as many as 18 morphometric parameters with highly significant differences, over half of which with *P* values <10⁻¹⁰ (after Bonferroni correction). When pair-wise comparisons were carried out between each of these two groups and the Claiborne group, eight parameters remained significant over all three comparisons (Table 5). These parameters include contraction, local bifurcation angle, and several diameter-dependent morphometrics (e.g., total dendritic surface and last bifurcation diameter). Only one parameter (parent-child diameter ratio) was significantly different between the three interlaboratory pair-wise comparisons and the CA3-CA1 comparison.

The best discriminating parameter between morphological classes (maximum branch order) appears to constitute two almost entirely nonoverlapping distributions from CA3 and CA1 (Table 4). Similarly, contraction seems to allow nearly perfect separations between the three reconstructing laboratories (Table 5). Thus, a two-dimensional scatter plot of these measurements should result in clear clusters grouped both by class and laboratory. Figure 4A confirms this expectation: reconstructing laboratories (represented by different shapes) are layered horizontally and perfectly separated (contraction values smaller than 0.9 for Turner cells, between 0.9 and 0.95 for Claiborne cells, and greater than 0.95 for Amaral cells). Morphological classes (represented by open vs. filled symbols) are grouped vertically and with minimal overlap (maximum branching order greater than 16 for CA1 cells, and smaller than or equal to 15 for CA3 cells, with only 5 outliers out of 117 neurons). A similar clustering can be observed in a two-dimensional scatter plot (Fig. 4B) of average branch diameter (separating laboratories) and topological asymmetry (separating morphological classes).

TABLE 4. Comparison between CA1 and CA3 Neurons Pooled from the Amaral, Turner, and Claiborne Groups (Thus, B3 and G1 Are Excluded)¹

Parameter	CA1	CA3	<i>P</i> value
Max branch order	23 ± 5.3	10 ± 2.2	6.3 · 10⁻¹⁷***
Remote bifurcation angle	55 ± 8.0	44 ± 8.4	5.5 · 10⁻⁰⁸***
Topological asymmetry	0.54 ± 0.049	0.47 ± 0.053	1.3 · 10⁻⁰⁷***
Soma surface	130 ± 110	430 ± 380	6.5 · 10⁻⁰⁶***
Max distance	730 ± 120	590 ± 140	4.9 · 10⁻⁰⁵***
Sholl distance	260 ± 50	210 ± 40	0.00020***
Max path distance	1100 ± 370	870 ± 390	0.00090***
Trees	4.6 ± 1.7	5.8 ± 1.7	0.0013**
Power correction	1.7 ± 0.13	1.5 ± 0.19	0.0020**
Parent-child ratio	0.85 ± 0.055	0.80 ± 0.088	0.015*
Rall's Power	1.3 ± 0.46	1.6 ± 0.46	0.037*
Local bifurcation angle	77 ± 16	68 ± 18	0.12
Diameter	0.63 ± 0.38	0.79 ± 0.45	0.19
Bifurcations	90 ± 27	80 ± 24	0.24
Branches	180 ± 55	160 ± 48	0.32
Last bifurcation diameter	0.60 ± 0.41	0.76 ± 0.45	0.35
Branch taper rate	-0.022 ± 0.027	-0.030 ± 0.039	0.39
Total volume	9000 ± 9500	15000 ± 13000	0.45
Unit taper rate	-0.049 ± 0.0050	-0.0081 ± 0.009	≥1
Height	730 ± 220	670 ± 180	≥1
Diameter threshold	0.60 ± 0.38	0.76 ± 0.51	≥1
Total length	16000 ± 6100	16000 ± 7900	≥1
Branch length	90 ± 23	95 ± 23	≥1
Total surface	31000 ± 20000	40000 ± 29000	≥1
Depth	280 ± 200	250 ± 74	≥1
Max tips	99 ± 30	98 ± 30	≥1
Contraction	0.84 ± 0.11	0.86 ± 0.13	≥1
Width	500 ± 210	530 ± 270	≥1
Daughter ratio	1.8 ± 0.48	1.8 ± 0.35	≥1
Hausdorff	1.5 ± 0.15	1.5 ± 0.13	≥1

¹Statistically significant parameters are bold.

*→ *P* ≤ 0.05.

**→ *P* ≤ 0.01.

***→ *P* ≤ 0.001.

To further assess the relative magnitude of the morphological differences between classes, between laboratories, and between other experimental parameters (e.g., age and preparation method), an additional analysis was run to compare the various subgroups of the Turner cells (T1.young, T1.old, T1.vivo, and T3) and the data sets excluded from the previous analysis, namely Gulyas CA1 cells (G1) and Barrionuevo CA3 cells (B3). Such a comparison constitutes a validation test, because these additional data sets (and the separated subgroups within T1) were not considered to characterize the morphometric differences discriminating between laboratories and between morphological classes. Figure 6 again shows an excellent separation between morphological classes based on the maximum branch order, independent of the laboratory of origin (e.g., note similar vertical clustering of B3 and T3, and of G1 and all T1 groups). Different laboratories are equally well separated horizontally, while differences in preparation method or age (T1.young vs. T1.vivo and T1.young vs. T1.old, respectively) resulted in no significant clustering in either of the two dimensions. Qualitatively similar scatter plots (not shown) were obtained for other pairs of significant parameters from Tables 4 and 5, respectively.

Both morphological differences between anatomical classes and reconstructing laboratories involve parameters that could affect the biophysical properties and the firing behavior of the neurons. To investigate this possibility, we used a computational model that could capture basic aspects of hippocampal pyramidal cell electrophysiology, while consisting of simple passive and active elements uniformly distributed over the whole structure (soma and dendrites) of all neurons (see also Vetter et al.,

TABLE 5. Comparison between Amaral and Turner Neurons (Pooled CA3 and CA1)¹

	A	T	<i>P</i> value
Contraction	0.98 ± 0.0065	0.75 ± 0.060	0***
Local bifurcation angle	54 ± 4.7	88 ± 7.3	3.5 · 10⁻¹⁷***
Diameter threshold	0.31 ± 0.022	0.70 ± 0.28	5.5 · 10⁻¹⁵***
Total volume	2800 ± 1600	13000 ± 11000	4.0 · 10⁻¹³***
Total surface	16000 ± 4000	41000 ± 24000	2.9 · 10⁻¹²***
Last bifurcation diameter	0.35 ± 0.077	0.67 ± 0.27	1.4 · 10⁻¹¹***
Diameter	0.39 ± 0.058	0.70 ± 0.25	9.2 · 10⁻¹¹***
Parent-child ratio	0.79 ± 0.079	0.86 ± 0.054	0.00015***
Branch taper rate	-0.0058 ± 0.0034	-0.040 ± 0.036	3.5 · 10 ⁻¹² ***
Soma surface	470 ± 350	93 ± 78	8.3 · 10 ⁻¹² ***
Max path distance	750 ± 130	1200 ± 400	9.1 · 10 ⁻¹² ***
Remote bifurcation angle	44 ± 6.2	56 ± 8.2	1.5 · 10 ⁻¹⁰ ***
Branch length	78 ± 7.6	100 ± 27	6.7 · 10 ⁻⁰⁹ ***
Hausdorff	1.6 ± 0.13	1.5 ± 0.13	6.8 · 10 ⁻⁰⁷ ***
Total length	13000 ± 2300	19000 ± 8000	8.5 · 10 ⁻⁰⁵ ***
Power correction	1.5 ± 0.19	1.70 ± 0.12	0.00046***
Max tips	110 ± 19	95 ± 34	0.0036**
Width	430 ± 230	580 ± 220	0.0042**
Height	780 ± 140	650 ± 240	0.060
Unit taper rate	-0.0090 ± 0.0060	-0.0050 ± 0.0080	0.15
Depth	210 ± 37	310 ± 210	0.20
Trees	5.3 ± 1.5	4.8 ± 2.0	0.35
Daughter ratio	1.9 ± 0.39	1.80 ± 0.42	0.90
Bifurcations	82 ± 14	91 ± 32	≥1
Max distance	660 ± 110	690 ± 170	≥1
Branches	170 ± 29	180 ± 65	≥1
Rall's Power	1.3 ± 0.18	1.32 ± 0.39	≥1
Topological asymmetry	0.51 ± 0.063	0.52 ± 0.056	≥1
Max branch order	18 ± 8.5	18 ± 6.9	≥1
Sholl distance	240 ± 36	240 ± 60	≥1

¹Statistically significant parameters are marked with asterisks. However, only parameters that are also simultaneously significant in the pair-wise comparisons between Amaral and Claiborne and between Turner and Claiborne are bold. Gray background indicates the only parameter that is bold both here and in Table 4.

*→ *P* ≤ 0.05.

**→ *P* ≤ 0.01.

***→ *P* ≤ 0.001.

2001; Krichmar et al., 2002). Thus, any biophysical difference observed in the electrophysiological simulations must be attributed to morphological variability. CA3 and CA1 pyramidal cells from the Amaral and Turner laboratories were stimulated by somatic current clamp, and exhibited a classic spiking behavior (Fig. 7). Two protocols were used, namely, equal (non-normalized) somatic current injection to each of the neurons, and somatic current injection normalized by each neuron's impedance (approximately resulting in an equal initial depolarization to all neurons). Both these protocols are widely used in computational and experimental neuroscience and have been shown to be sensitive to morphological variability in hippocampal pyramidal cells (Nasuto et al., 2001; Krichmar et al., 2002).

When the firing rate in response to equal current injection was pair-wise compared in the four groups (A1, T1, A3, and T3), the statistical differences were very highly significant between anatomical classes (A1 vs. A3 and T1 vs. T3) and nonsignificant between reconstructing laboratories (A1 vs. T1 and A3 vs. T3). Interestingly, the measurements of impedance also exhibited the same patterns (Fig. 8A,B). As a consequence, upon normalization of the current injection by impedance, firing frequencies were significantly different both between anatomical classes and between reconstructing laboratories (Fig. 8C). However, in this protocol, the statistical differences between reconstructing laboratories were considerably more highly significant than those between anatomical classes ($\sim 10^{-7}$ vs. $\sim 10^{-2}$). A scatter plot of firing frequencies under equal and normalized injection conditions (Fig. 9) once again

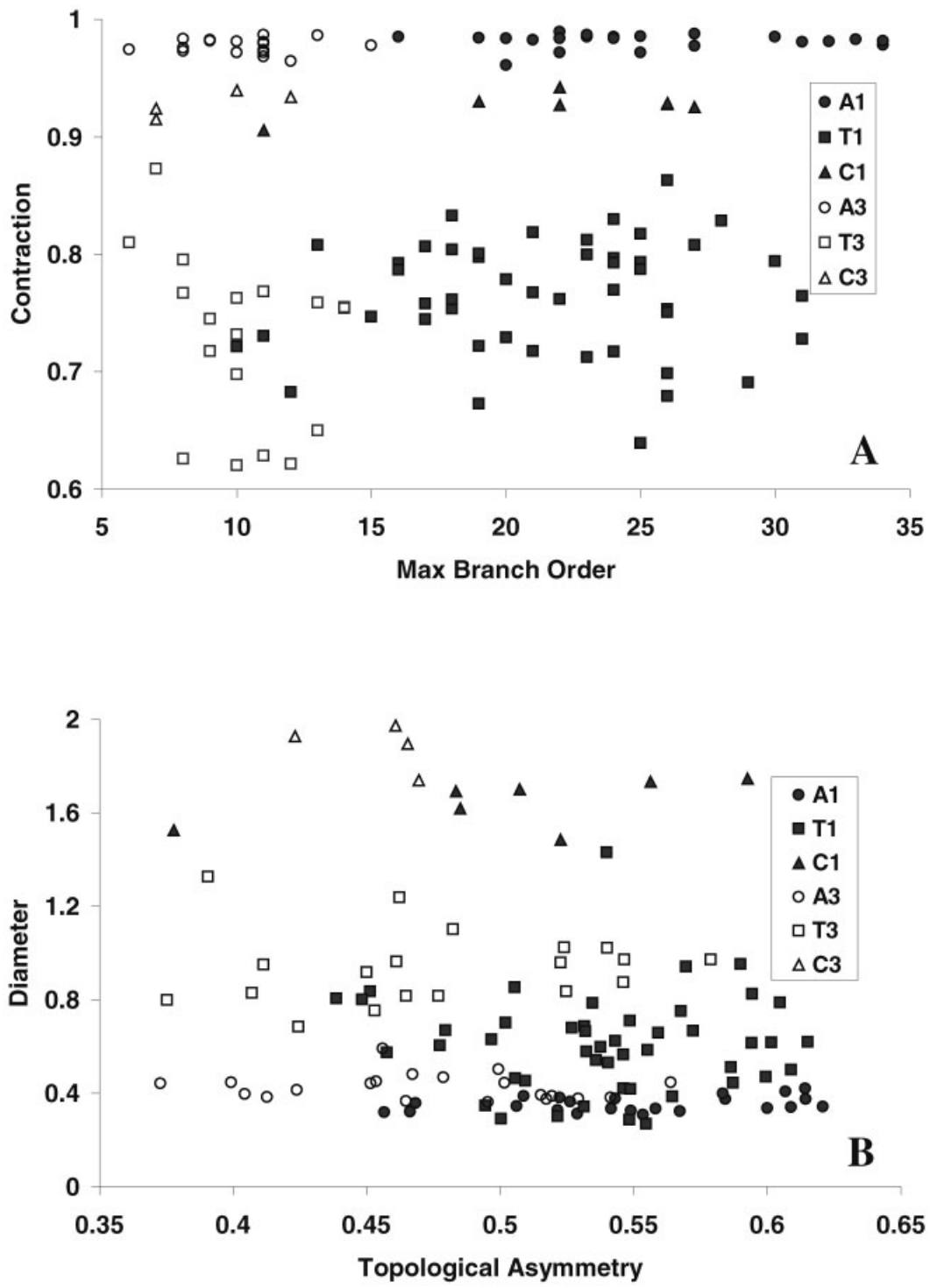


Fig. 4. Two-dimensional scatter plots of pairs of morphometric parameters. Full and hollow shapes represent CA1 and CA3 neurons, respectively. Each archive is associated to a unique shape (Amaral, circles; Turner, squares; Claiborne, triangles). **A**: Contraction versus maximum branch order. **B**: Diameter versus topological asymmetry.

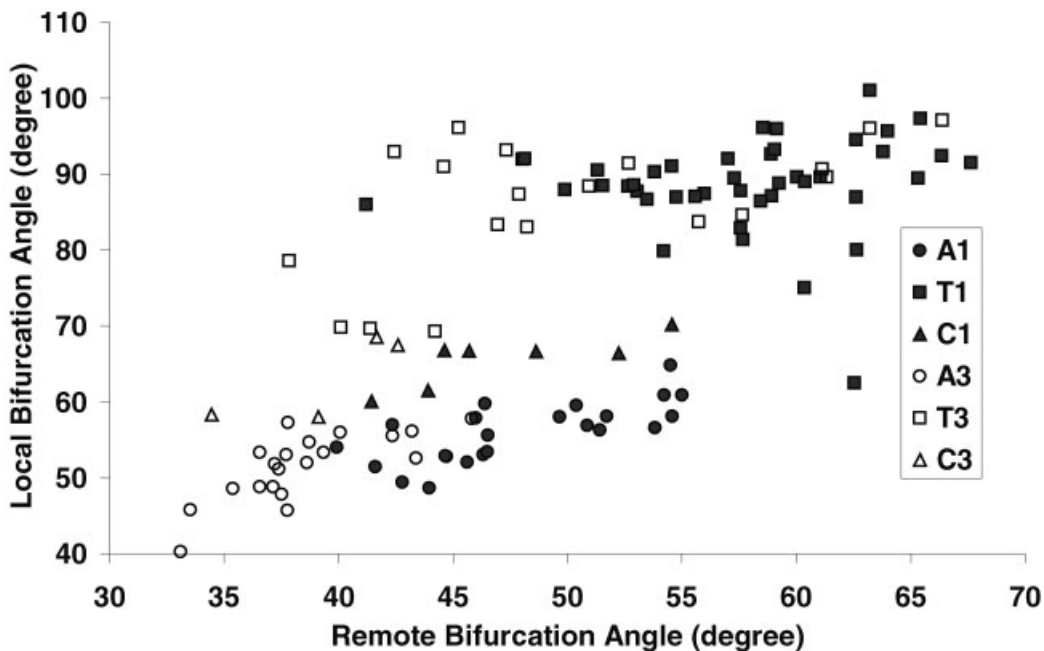


Fig. 5. Two-dimensional scatter plot of local vs. remote bifurcation angle. Symbols are as in Figure 4.

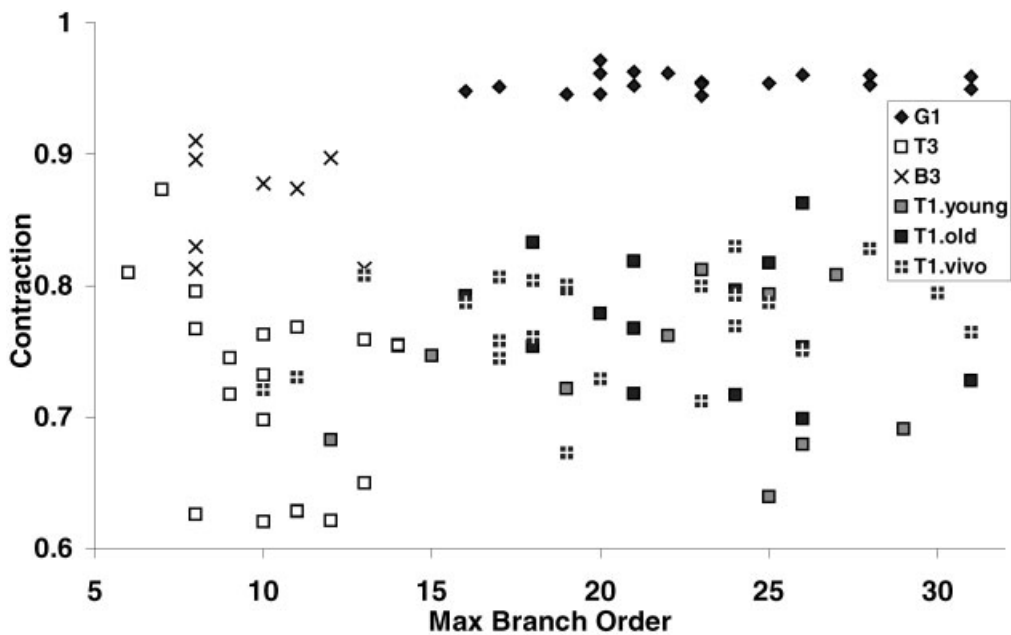


Fig. 6. "Validation" scatter plot of contraction versus maximum branch order measured from (sub)groups that were not used for the statistical results. Filled and open shapes represent CA1 and CA3 neurons, respectively. Each archive is associated to a unique shape, with Turner subgroups distinguished by filling patterns.

shows excellent differential separation of neurons by anatomical class (CA3 on the left, CA1 on the right) and by reconstructing laboratory (Amaral on the top, Turner on the bottom).

An important question regarding the biophysical basis of such firing frequency differences. In particular, the different response to normalized current of cells from the same class but different laboratories could

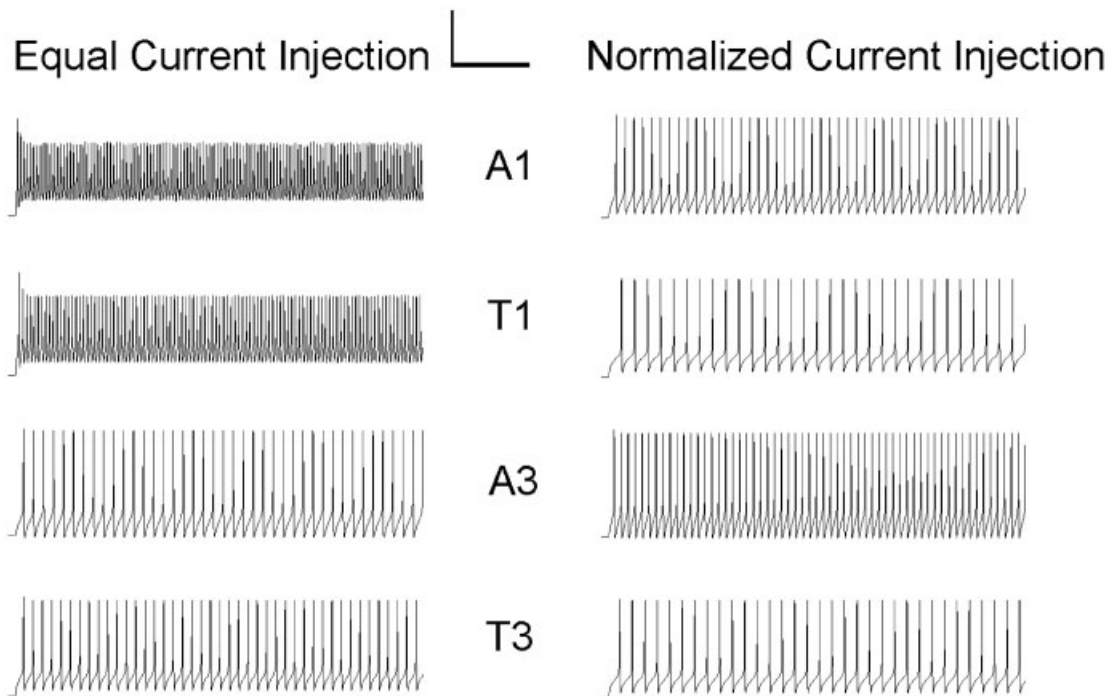


Fig. 7. Examples of simulated spike traces from the uniform active model in response to equal current injection (0.55 nA, left) and impedance-normalized current injection (6.5 nA divided by the impedance value at 100 Hz, in M Ω , right). The four traces correspond to

Amaral CA1 cell CD2351 (A1), Turner CA1 cell n422t (T1), Amaral CA3 cell C62563 (A3), and Turner CA3 cell l16t (T3). Scale bars = 50 mV (vertical); 100 msec (horizontal).

reflect a shift in the relationship between firing rate and normalized injected current (related to the sensitivity of the neurons) or a difference in f-IZ slope (corresponding to the gain of the neurons), or both. Measurement of slope and intercept of the f-IZ curves by linear regression around the normalized stimulation value for each neuron indicated that the observed difference in firing rate between laboratories is solely due to an f-IZ shift (Fig. 10). In particular, intercept values were dramatically different both between the A1 and T1 groups ($P < 1.7 \times 10^{-7}$) and the A3 and T3 groups ($P < 3.1 \times 10^{-7}$), while slope values were not ($P > 0.45$ in either case). Of interest, a change in f-IZ slope is in contrast observed between cells of different classes (A1–A3: $P < 8.1 \cdot 10^{-8}$; T1–T3: $P < 3.3 \cdot 10^{-4}$). Thus, firing rate differences between classes and between laboratories appear to be consequences of complementary mechanisms. This point is also illustrated in Figure 10, with the clear horizontal and vertical separations between anatomical classes and reconstructing laboratories, respectively.

Finally, because dendritic diameter is a major determinant of the longitudinal gradient of membrane potential, and as such is critically important for spike initiation, all discrepancies in firing frequency might be in principle due to differences in diameter measurements (Table 5). To test this possibility, firing frequency in response to stimuli normalized by input impedance at 100 Hz were remeasured after either additive or multiplicative diameter normalization (see Materials and Methods section). In both cases, however, all interclass and interlaboratory differences remained at the same or higher level of statistical significance as reported in Figure 8C.

DISCUSSION

The variability of dendritic morphology is widely investigated in neuroscience (Ascoli, 1999; Hausser et al., 2000; Koch and Segev, 2000; van Pelt, 2002). Three types of morphological variability emerge from the available reconstructions of rat hippocampal pyramidal cells: (1) intrinsic variability within a class and experimental group (i.e., two neurons of each pair in Fig. 1); (2) class-specific differences between CA1 and CA3 (left and right pairs of columns in Fig. 1); and (3) laboratory-specific differences (variability among pairs of neurons within columns in Fig. 1). The major finding of this work is that the laboratory-specific variability is of the same order of magnitude of the class-specific one, and significantly greater than the intrinsic variability.

Various morphological reports are often difficult to compare because they use different morphometrics. In this study, quantitative analysis was based on an exhaustive array of 30 parameters. This set included all measurements typically considered to characterize dendritic morphology, with the additional transformation of relational analyses (e.g., Sholl-like plots of segment numbers vs. path distance) into scalar values (Sholl distance) suitable for a direct statistical comparison. Two distinct subsets of parameters emerged with remarkably minimal overlap: a group of 11 parameters (Table 4) that significantly separate CA1 and CA3 pyramidal neurons; and a group of 8 parameters (Table 5) that significantly separate different reconstructing laboratories.

The parameters discriminating between morphological classes mostly represent global structural informa-

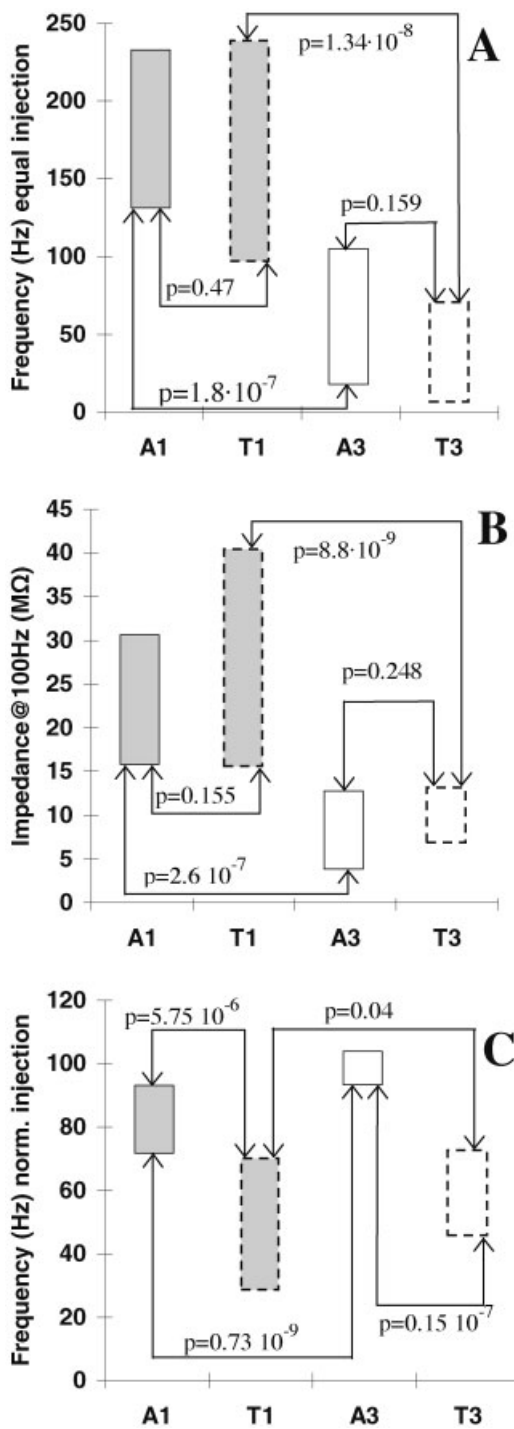


Fig. 8. Variability and pair-wise comparisons of simulated electrophysiological properties of A1, T1, A3, and T3 cells. For each group, floating columns represent a range of two standard deviations centered at the mean. **A:** Firing frequency in response to equal current injection. **B:** Impedance at 100 Hz measured at the soma. **C:** Firing frequency in response to current injection normalized by impedance.

tion, such as the maximum number of bifurcations and Euclidian distance between soma and dendritic terminations, and the angle between a bifurcation and the

next two bifurcations or terminations. A minority (less than one third) of the parameters found to differ between CA3 and CA1 pyramidal cells depend on branch diameter (parent-child ratio, Rall's power, power correction). These parameters, which are complex *functions* of diameters, such as diameter ratios, are not the most highly significant in this group but are robustly present across several data sets and experimental conditions. Many of the global parameters have been reported previously to discriminate between CA3 and CA1 neurons (e.g., Cannon et al., 1999). In contrast, this article is the first report of the more subtle diameter-dependent, class-specific differences. These observations may help explain the different electrotonic, electrophysiological, and biophysical properties of CA3 and CA1 pyramidal cells (Fig. 7; also Carnevale et al., 1997; Vetter et al., 2001; Migliore and Shepherd, 2002).

Unlike the class-specific differences, the parameters that significantly vary among reconstructing laboratories mainly represent local information, such as contraction (a measure of dendritic meandering), the angle between a bifurcation and the two immediately adjacent tracing points, and several diameter-dependent parameters (e.g., average branch diameter, and last bifurcation diameter). In contrast to the previous group of morphometric parameters, a majority (more than two thirds) of the parameters that significantly differ among laboratories depend on diameter (Table 5).

Given the relatively small sample size, and the heterogeneous experimental conditions across and within laboratories (e.g., strain, age, preparation protocols, reconstruction system, human operator), it is difficult to tease out individual statistical influences of a priori conditions on the resulting morphological data. CA1 pyramidal neurons in T1.young and A1, for instance, differ in gender, reconstruction system, and operator, but have same strain, preparation protocol, and morphological class. In addition, analyzing differences between laboratories is particularly difficult because typical published protocols do not explicitly describe all subtle steps during the collection and preparation of the data. Nevertheless, qualitative indications can be inferred from the available samples. For example, T1 subgroups are separated by age, preparation method, and animal strain (Table 1), but only minimal differences are found among them. Conversely, T1.vivo and G1 neurons have same gender, preparation method, and age but differ in strain, reconstruction system, and operator, and they present striking morphological differences (Figs. 2, 3, 6). Strain differences are unlikely to be responsible for laboratory-specific variability, because the same parameters discriminating laboratories are significantly different between groups of neurons from the same strain (e.g., Amaral, Claiborne, and Barrionuevo). In addition, strain (as well as age and preparation method) differences are considerably washed out when data from various groups are pooled together within the same laboratory (Amaral, Turner, and Claiborne: Table 5). The same parameters that significantly separate these "super-classes" also discriminate the remaining laboratories (Barrionuevo and Gulyas: Figs. 3, 6).

One possibility is that different laboratories might have specific biases for various regions of the hippocampus, therefore collecting unbalanced proportions of different

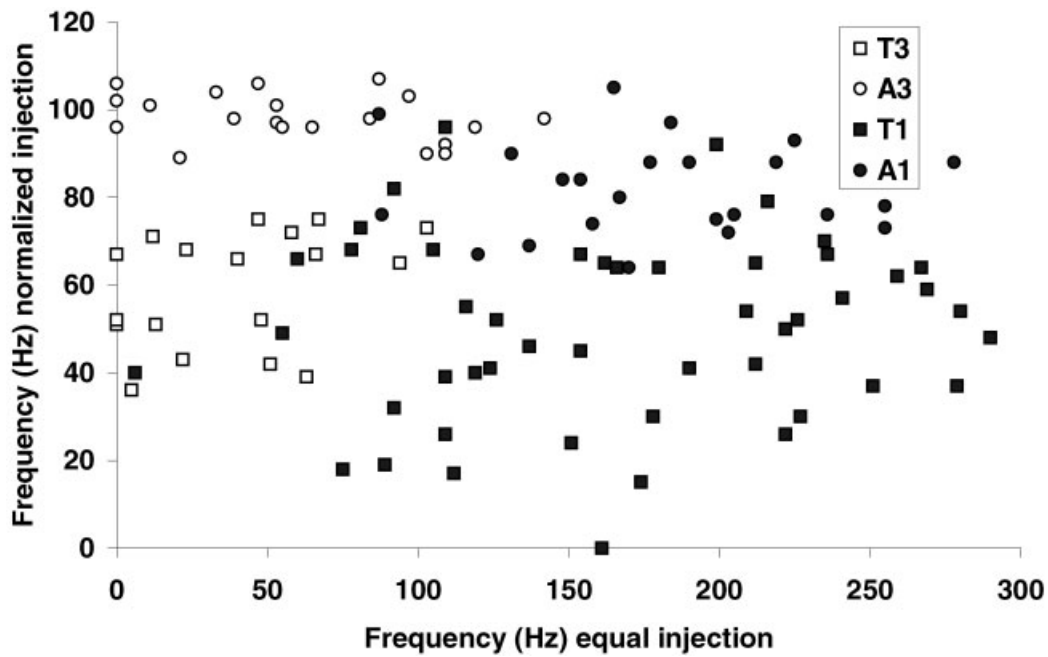


Fig. 9. Two-dimensional scatter plot of firing frequencies in response to equal and normalized current injections. Filled and open shapes represent CA1 and CA3 neurons, respectively. Each archive is associated to a unique shape.

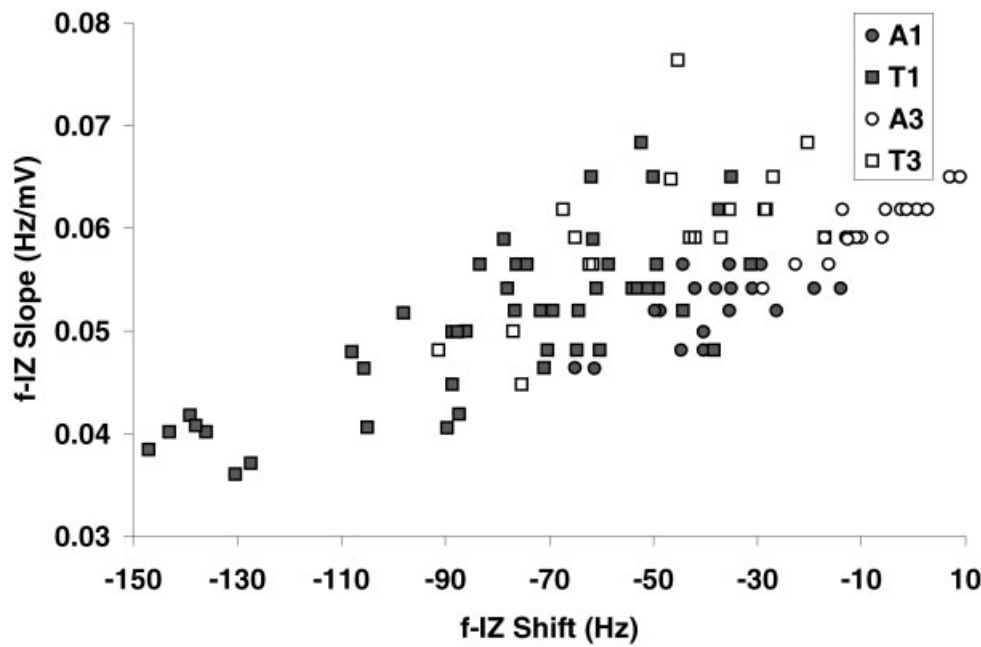


Fig. 10. Two-dimensional scatter plot of the slope and intercept (“shift”) of the firing frequency–normalized stimulating injection (f-IZ) relationship for neurons from different regions and archives. Current

injections were normalized by somatic impedance at 100 Hz. Filled and open shapes represent CA1 and CA3 neurons, respectively. Each archive is associated to a unique shape.

morphological subclasses of neurons (e.g., CA3a,b,c). Nevertheless, the two largest archives (Turner and Amaral) contain precise information on the location of the reconstructed cells, which are equally and uniformly distrib-

uted (Ishizuka et al., 1995; Turner et al., 1995; Pyapali et al., 1998). In addition, while specific subclasses are recognized in CA3 (Turner et al., 1995), the CA1 region is more homogeneous (Ishizuka et al., 1995). In our analysis, in-

terlaboratory differences discriminated equally well neurons from CA3 and CA1 (and from the two classes pooled together; Table 5).

On the basis of these considerations, we are inclined to attribute the major causes of the morphological differences among laboratories to (1) experimental details beyond animal strain, age, and intracellular injection protocol; (2) individual operators; and (3) specific reconstruction system (e.g., microscope optics and stage mounting, settings of the tracing software).

Contraction, for example, measures the amount of dendritic meandering. This parameter is likely affected by dehydration-induced shrinkage. Claiborne's laboratory introduced the use of glycerol concentration gradients during the final washing stage before slide mounting, to limit dendritic shrinkage (Claiborne et al., 1990). Amaral's lab additionally discontinued the use of filter paper, with the same goal. These details partly explain the low contraction values of Claiborne's cells relative to Turner's, and the lowest values of Amaral's (Table 5; Fig. 4). Contraction also critically depends on the number of tracing points. At a lower limit, dendritic points are traced at every turn or detectable change of diameter. The upper limit, however, is largely an operator's arbitrary choice. Higher numbers of tracing points may result in higher contraction values. Turner's cells have an order of magnitude more tracing points than Amaral's, further explaining this particular difference.

Branch diameter is affected by the reconstruction system settings. In all these data sets, diameter values are discretized. The specific values are preset in commercial software packages, depending on the lens magnification (e.g., for *NeuroLucida*, see www.microbrightfield.com). While these issues are generally discussed and acknowledged (e.g., Ishizuka et al., 1995, www.utsa.edu/claibornelab), operators' individual heuristics also are at play. For example, 63 \times /100 \times oil objectives, adopted in all these studies, make dendritic spines visible. Because spines are typically *not* reconstructed along the branches, operators may chose to trace dendrites at the base of the spine necks or as encompassing surfaces at the top of the spine heads (underestimating or overestimating, respectively, the resulting average diameter from its "true" value).

The influences of subtle differences in the microscope and reconstruction system, and of the operator identity, are also highlighted by recent anecdotal reports on the tracing variability of the same neuron, from the same slide. Significant morphological differences were found between reconstructions obtained on the same system by two different operators (Jaeger, 2001), or by the same operator on two different systems (Kaspirzhny et al., 2002). Each slide set is also obviously unique, because of subtle experimental procedure variations that are exceedingly impractical to record, such as exact animal housing conditions.

Computational models of pyramidal cells are increasingly making use of experimentally reconstructed morphologies. These include studies of the structural and biophysical bases of electrophysiological behavior (e.g., Vetter et al., 2001; Krichmar et al., 2002, Schaefer et al., 2003), synaptic and network plasticity (van Ooyen and van Pelt, 1996), and neuronal growth and orientation (Samsonovich and Ascoli, 2003). Here, we show that both class-dependent and laboratory-dependent

morphological differences can selectively affect simulated biophysical properties. Firing rates in response to current clamp, as well as impedance values, significantly differ between anatomical classes but not between laboratories. However, in response to current clamp normalized by impedance, firing rate differences are considerably more highly significant between laboratories than between classes (Fig. 8). In this case, two complementary mechanisms appear to be responsible for the firing rate variability: while differences between laboratories are due to a shift of the relationship between firing rate and injected current, differences between anatomical classes are due to a change in f-I slope (Fig. 10). These results indicate that particular attention needs to be paid when biophysical models expected to be sensitive to dendritic morphology are ported across data sources. Laboratory-specific differences could affect the results of these models even more than differences between morphological classes. Normalizing diameter values may not be sufficient or even useful, as the differences in firing rates most likely emerge from more complex and/or subtle combinations of parameters.

The issue of "morphological noise" in digital reconstructions has been extensively discussed (Ascoli et al., 2001; Kaspirzhny et al., 2002; Turner et al., 2002). This report shows that "data quality" cannot be quantified by a single parameter. For example, within a data set, reconstructed neurons can have precise spatial coordinates (e.g., due to reduced shrinkage) and less-precise diameter information (e.g., due to constraints of the reconstruction software). The choice of data to use in particular modeling efforts should be critically considered based on the scientific question at stake. Similar care should be taken when comparing morphological analyses from several laboratories investigating differences between neuronal classes. Local and diameter-dependent parameters can depend more heavily on the reconstructing laboratory than on the morphological class. Nonetheless, here we characterized several laboratory-*independent* differences between CA3 and CA1, which mainly consist of global geometrical properties, and appear to be robust relative to subtle and difficult-to-control experimental details.

ACKNOWLEDGMENTS

We thank Drs. David Amaral, German Barrionuevo, Thomas Brown, Gyorgy Buzsaki, Nicholas Carnevale, Brenda Claiborne, Darrell Henze, Attila Gulyas, Norio Ishizuka, Manuel Megias, Gowri Pyapali, Dennis Turner, and their collaborators, for their willingness to share data files constituting many years of experimentation. We also thank Mr. Guido Cervone for writing and providing a machine learning program used for exploratory data analysis in the preliminary phases of this project (relevant technical details will be reported elsewhere). We also thank all members of the Computational Neuroanatomy Group for countless discussions, Drs. Avrama Blackwell, Nancy Desmond, Andrea Foulkes, and Jeff Krichmar for invaluable advice, and Dr. Ann Butler for useful feedback on an earlier version of the article.

LITERATURE CITED

- Anderton BH, Callahan L, Coleman P, Davies P, Flood D, Jicha GA, Ohm T, Weaver C. 1998. Dendritic changes in Alzheimer's disease and factors that may underlie these changes. *Prog Neurobiol* 55:595–609.
- Ascoli GA. 1999. Progress and perspective in computational neuroanatomy. *Anat Rec* 257:195–207.
- Ascoli GA. 2002. Neuroanatomical algorithms for dendritic modelling. *Network* 13:247–260.
- Ascoli GA, Krichmar JL, Nasuto SJ, Senft SL. 2001. Generation, description and storage of dendritic morphology data. *Philos Trans R Soc Lond B Biol Sci* 356:1131–1145.
- Benjamini Y, Hochberg Y. 1995. Controlling the false discovery rate: a practical and powerful approach to multiple testing. *JR Stat Soc Ser B* 57:289–300.
- Bilkey DK, Schwartzkroin PA. 1990. Variation in electrophysiology and morphology of hippocampal CA3 pyramidal cells. *Brain Res* 514:77–83.
- Bulinski JC, Ohm T, Roder H, Spruston N, Turner DA, Wheal HV. 1998. Changes in dendritic structure and function following hippocampal lesions: correlations with developmental events? *Prog Neurobiol* 55:641–650.
- Buzsaki G. 1989. Two-stage model of memory trace formation: a role for "noisy" brain states. *Neuroscience* 31:551–570.
- Cannon RC, Turner DA, Pyapali GK, Wheal HV. 1998. An on-line archive of reconstructed hippocampal neurons. *J Neurosci Methods* 84:49–54.
- Cannon RC, Wheal HV, Turner DA. 1999. Dendrites of classes of hippocampal neurons differ in structural complexity and branching patterns. *J Comp Neurol* 413:619–633.
- Capowski JJ. 1983. An automatic neuron reconstruction system. *J Neurosci Methods* 8:353–364.
- Carnevale NT, Tsai KY, Claiborne BJ, Brown TH. 1997. Comparative electrotonic analysis of three classes of rat hippocampal neurons. *J Neurophysiol* 78:703–720.
- Clairborne BJ, Amaral DG, Cowan WM. 1990. Quantitative three-dimensional analysis of granule cell dendrites in the rat dentate gyrus. *J Comp Neurol* 302:206–219.
- Collin C, Miyaguchi K, Segal M. 1997. Dendritic spine density and LTP induction in cultured hippocampal slices. *J Neurophysiol* 77:1614–1623.
- Colling SB, Man WD, Draguhn A, Jefferys JG. 1996. Dendritic shrinkage and dye-coupling between rat hippocampal CA1 pyramidal cells in the tetanus toxin model of epilepsy. *Brain Res* 741:38–43.
- Desmond NL, Levy WB. 1997. Ovarian steroidal control of connectivity in the female hippocampus: an overview of recent experimental findings and speculations on its functional consequences. *Hippocampus* 7:239–245.
- Donohue DE, Scorcioni R, Ascoli GA. 2002. Generation and description of neuronal morphology using L-Neuron: a case study. In: Ascoli GA, editor. *Computational neuroanatomy*. Totowa: Humana Press. p 49–70.
- Duffell SJ, Soames AR, Gunby S. 2000. Morphometric analysis of the developing rat brain. *Toxicol Pathol* 28:157–163.
- Fiala JC, Harris KM. 2001. Extending unbiased stereology of brain ultrastructure to three-dimensional volumes. *J Am Med Inform Assoc* 8:1–16.
- Gardner D, and 31 other authors. 2003. Towards effective and rewarding data sharing. *Neuroinformatics* 1:289–296.
- Glaser JR, Glaser EM. 1990. Neuron imaging with neurolucida—a PC-based system for image combining microscopy. *Comput Med Imaging Graph* 14:307–317.
- Gluck MA. 1996. Computational models of hippocampal function in memory. *Hippocampus* 6:565–566.
- Hasselmo ME, Wyble BP. 1997. Free recall and recognition in a network model of the hippocampus: simulating effects of scopolamine on human memory function. *Behav Brain Res* 89:1–34.
- Hausser M, Spruston N, Stuart GJ. 2000. Diversity and dynamics of dendritic signaling. *Science* 290:739–744.
- Henze DA, Cameron WE, Barrionuevo G. 1996. Dendritic morphology and its effects on the amplitude and rise-time of synaptic signals in hippocampal CA3 pyramidal cells. *J Comp Neurol* 369:331–344.
- Hines ML, Carnevale NT. 1997. The NEURON simulation environment. *Neural Comput* 9:1179–1209.
- Hines ML, Carnevale NT. 2001. NEURON: a tool for neuroscientists. *Neuroscientist* 7:123–135.
- Irwin SA, Idupulapati M, Gilbert ME, Harris JB, Chakravarti AB, Rogers EJ, Crisostomo RA, Larsen BP, Mehta A, Alcantara CJ, Patel B, Swain RA, Weiler IJ, Oostra BA, Greenough WT. 2002. Dendritic spine and dendritic field characteristics of layer V pyramidal neurons in the visual cortex of fragile-X knockout mice. *Am J Med Genet* 111:140–146.
- Ishizuka N, Cowan WM, Amaral DG. 1995. A quantitative analysis of the dendritic organization of pyramidal cells in the rat hippocampus. *J Comp Neurol* 362:17–45.
- Jaeger D. 2001. Accurate reconstruction of neuronal morphology. In: De Schutter E, editor. *Computational neuroscience: realistic modeling for experimentalists*. Boca Raton: Lewis Publishers, Inc. p 159–178.
- Kaspirzhny AV, Gogan P, Horcholle-Bossavit G, Tyc-Dumont S. 2002. Neuronal morphology data bases: morphological noise and assessment of data quality. *Network* 13:357–380.
- Kaufmann EW, Moser WH. 2000. Dendritic anomalies in disorders associated with mental retardation. *Cereb Cortex* 10:981–991.
- Koch C, Segev I. 2000. The role of single neurons in information processing. *Nat Neurosci* 3:1171–1177.
- Krichmar J, Nasuto S, Scorcioni R, Washington S, Ascoli G. 2002. Influence of dendritic morphology on CA3 pyramidal cell electrophysiology. *Brain Res* 941:11–28.
- Larkman A, Mason A. 1990. Correlations between morphology and electrophysiology of pyramidal neurons in slices of rat visual cortex. I. Establishment of cell classes. *J Neurosci* 10:1407–1414.
- Lazarewicz MT, Boer-Iwema S, Ascoli GA. 2002a. Practical aspects in anatomically accurate simulations of neuronal electrophysiology. In: Ascoli GA, editor. *Computational neuroanatomy*. Totowa: Humana Press. p 127–148.
- Lazarewicz MT, Migliore M, Ascoli GA. 2002b. A new bursting model of CA3 pyramidal cell physiology suggests multiple locations for spike initiation. *Biosystems* 67:129–137.
- Levy WB. 1996. A sequence predicting CA3 is a flexible associator that learns and uses context to solve hippocampal-like tasks. *Hippocampus* 6:579–590.
- Marr D. 1971. Simple memory: a theory for archicortex. *Philos Trans R Soc Lond B Biol Sci* 262:23–81.
- McNaughton BL, Barnes CA, Gerrard JL, Gothard K, Jung MW, Kniermim JJ, Kudrimoti H, Qin Y, Skaggs WE, Suster M, Weaver KL. 1996. Deciphering the hippocampal polyglot: the hippocampus as a path integration system. *J Exp Biol* 199:173–185.
- Megias M, Emri Z, Freund TF, Gulyas AI. 2001. Total number and distribution of inhibitory and excitatory synapses on hippocampal CA1 pyramidal cells. *Neuroscience* 102:527–540.
- Migliore M, Shepherd GM. 2002. Emerging rules for the distributions of active dendritic conductances. *Nat Rev Neurosci* 3:362–370.
- Migliore M, Cook EP, Jaffe DB, Turner DA, Johnston D. 1995. Computer simulations of morphologically reconstructed CA3 hippocampal neurons. *J Neurophysiol* 73:1157–1168.
- Muller D, Nikonenko I, Jourdain P, Alberi S. 2002. LTP, memory and structural plasticity. *Curr Mol Med* 2:605–611.
- Nasuto SJ, Knape RM, Krichmar JL, Ascoli GA. 2001. Relation between neuronal morphology and electrophysiology the Kainate lesion model of Alzheimer's Disease. *Neurocomputing* 38-40:1477–1487.
- Paré D, Lang EJ, Destexhe A. 1998. Inhibitory control of somatodendritic interactions underlying action potentials in neocortical pyramidal neurons in vivo: an intracellular and computational study. *Neuroscience* 84:377–402.
- Poirazi P, Brannon T, Mel BW. 2003. Arithmetic of subthreshold synaptic summation in a model CA1 pyramidal cell. *Neuron* 37:977–987.
- Pokorny J, Yamamoto T. 1981. Postnatal ontogenesis of hippocampal CA1 area in rats. I. Development of dendritic arborization in pyramidal neurons. *Brain Res Bull* 7:113–120.
- Pyapali GK, Turner DA. 1994. Denervation-induced dendritic alterations in CA1 pyramidal cells following kainic acid hippocampal lesions in rats. *Brain Res* 652:279–290.
- Pyapali GK, Turner DA. 1996. Increased dendritic extent in hippocampal CA1 neurons from aged F344 rats. *Neurobiol Aging* 17:601–611.
- Pyapali GK, Sik A, Penttonen M, Buzsaki G, Turner DA. 1998. Dendritic properties of hippocampal CA1 pyramidal neurons in the rat: intracellular staining in vivo and in vitro. *J Comp Neurol* 391:335–352.
- Rolls ET. 1996. A theory of hippocampal function in memory. *Hippocampus* 6:601–620.
- Samsonovich AV, Ascoli GA. 2003. Statistical morphological analysis of

- hippocampal principal neurons indicates cell-specific repulsion of dendrites from their own cell. *J Neurosci Res* 71:173–187.
- Schaefer AT, Larkum ME, Sakmann B, Roth A. 2003. Coincidence detection in pyramidal neurons is tuned by their dendritic branching pattern. *J Neurophysiol* 89:3143–3154.
- Scheibel AB. 1980. Morphological correlates of epilepsy: cells in the hippocampus. *Adv Neurol* 27:49–61.
- Scorcioni R, Ascoli GA. 2001. Algorithmic extraction of morphological statistics from electronic archives of neuroanatomy. *Lect Notes Comp Sci* 2084:30–37.
- Shapiro ML, Eichenbaum H. 1999. Hippocampus as a memory map: synaptic plasticity and memory encoding by hippocampal neurons. *Hippocampus* 9:365–384.
- Shetty AK, Turner DA. 1995. Enhanced cell survival in fetal hippocampal suspension transplants grafted to adult rat hippocampus following kainate lesions: a three-dimensional graft reconstruction study. *Neuroscience* 67:561–582.
- Swann JW, Al-Noori S, Jiang M, Lee CL. 2000. Spine loss and other dendritic abnormalities in epilepsy. *Hippocampus* 10:617–625.
- Turner DA, Li XG, Pyapali GK, Ylinen A, Buzsaki G. 1995. Morphometric and electrical properties of reconstructed hippocampal CA3 neurons recorded in vivo. *J Comp Neurol* 356:580–594.
- Turner DA, Cannon RC, Ascoli GA. 2002. Web-based neuronal archives: neuronal morphometric and electrotonic analysis. In: Kotter R, editor. *Neuroscience databases*. Boston: Kluwer Academic Publishers. p 81–98.
- van Ooyen A, van Pelt J. 1996. Complex periodic behaviour in a neural network model with activity-dependent neurite outgrowth. *J Theor Biol* 179:229–242.
- van Pelt J. 2002. Quantitative neuroanatomy and neuroinformatics. *Network* 13:243–245.
- Vetter P, Roth A, Hausser M. 2001. Propagation of action potentials in dendrites depends on dendritic morphology. *J Neurophysiol* 85:926–937.
- Wasowicz I, Kishikawa M, Sakae M, Kawaguchi S, Kondo H, Kashima K, Wasowicz M, Yokoyama S, Nakayama I. 1996. Quantitative age-related changes in apical dendrites and dendritic spines of CA1 pyramidal neurons among senescence accelerated mice (SAMP1TA/Ngs). *Mech Ageing Dev* 90:63–73.
- Wolf E, Birinyi A, Pomahazi S. 1995. A fast 3-dimensional neuronal tree reconstruction system that uses cubic polynomials to estimate dendritic curvature. *J Neurosci Methods* 63:137–145.